

## Conference paper

Mariia Lemishka\*, Jiri Dedecek, Kinga Mlekodaj, Zdenek Sobalik, Stepan Sklenak and Edyta Tabor

# Speciation and siting of divalent transition metal ions in silicon-rich zeolites. An FTIR study

<https://doi.org/10.1515/pac-2018-1228>

**Abstract:** Speciation and location of  $\text{Co}^{2+}$ ,  $\text{Mn}^{2+}$  and  $\text{Ni}^{2+}$  in the extraframework positions of the dehydrated zeolite matrix of ferrierite structure were studied in detail using FTIR spectroscopy of antisymmetric T–O–T vibrations of the zeolite framework.  $\text{Me}^{2+}$ -ferrierites were prepared by the ion exchange of the  $\text{NH}_4^-$  and Na-zeolite forms and by impregnation of the  $\text{NH}_4$  form. Bare  $\text{Me}^{2+}$  occupies all three known cationic sites in dehydrated cationic zeolite. The wavenumbers of bands of individual cations in individual sites were identified. At low  $\text{Me}^{2+}$  loadings ( $\text{Me}^{2+}/\text{Al} < 0.15$ ),  $\text{Me}^{2+}$  replaces two protonic sites and exclusively bare  $\text{Me}^{2+}$  is present in dehydrated samples. Sets of such samples were employed for the estimation of extinction coefficients of  $\text{Co}^{2+}$ ,  $\text{Mn}^{2+}$  and  $\text{Ni}^{2+}$  in cationic sites. These coefficients differ for individual cations but are the same for a cation at different sites. Ion exchange to the  $\text{NH}_4$  form allows preparation of samples with maximum possible loading of bare  $\text{Me}^{2+}$  only for  $\text{Co}^{2+}$ . In the case of  $\text{Mn}^{2+}$ , exchange to the Na-parent zeolite or impregnation is required for this purpose while samples with maximum loading by bare  $\text{Ni}^{2+}$  can be prepared only by impregnation.

**Keywords:** Brønsted acid; cobalt; infrared; manganese; nickel; SSC-2018; transition-metal catalysis; zeolites.

## Introduction

Zeolites are key materials for chemical production (heterogeneous catalysis, gas separation and purification). Zeolites are crystalline microporous aluminosilicate molecular sieves formed by  $\text{SiO}_4$  and  $\text{AlO}_4^-$  tetrahedra sharing their corners [1, 2]. The isomorphous substitution of silicon by aluminum in the zeolite framework introduces a negative charge which has to be balanced by extraframework positively charged species. The extraframework protons, cations or cationic species can play the role of active sites for both acid- and redox-catalyzed reactions. The huge variability of extraframework active sites in zeolites: Brønsted and Lewis acid sites, cation basic sites, redox cation and oxidic sites, makes it possible to tune their properties to the requirements of the catalytic reactions. This, together with large internal surface, high mechanical and thermal stability and rather simple and economic large-scale production results in the fact that zeolites represent currently the widest and most important group of industrial catalysts [2, 3]. They are used as catalysts in a wide range of acid-catalyzed reactions for the transformations of hydrocarbons in the petrochemical industry and

**Article note:** A collection of invited papers based on presentations at the 13<sup>th</sup> International Conference on Solid State Chemistry (SSC-2018), Pardubice, Czech Republic, September 16–21, 2018.

**\*Corresponding author: Mariia Lemishka**, J. Heyrovský Institute of Physical Chemistry of the Czech Academy of Sciences, Dolejškova 2155/3, CZ-182 23 Prague 8, Czech Republic; and University of Pardubice, Pardubice, Czech Republic, e-mail: mariia.lemishka@jh-inst.cas.cz

**Jiri Dedecek, Kinga Mlekodaj, Zdenek Sobalik, Stepan Sklenak and Edyta Tabor:** J. Heyrovský Institute of Physical Chemistry of the Czech Academy of Sciences, Dolejškova 2155/3, CZ-182 23 Prague 8, Czech Republic

 © 2019 IUPAC & De Gruyter. This work is licensed under a Creative Commons Attribution-NonCommercial-NoDerivatives 4.0 International License. For more information, please visit: <http://creativecommons.org/licenses/by-nc-nd/4.0/>

Brought to you by | provisional account  
Unauthenticated  
Download Date | 1/10/20 10:15 AM

synthesis of fine chemicals [4, 5]. Metallozeolites with metal ion cationic species represent redox catalysts for NO/NO<sub>x</sub> elimination from diesel exhausts and N<sub>2</sub>O abatement [6]. Recently, zeolites were reported to be promising catalysts in the utilization of biomass [7], conversion of methane to oxygen-containing products and utilization of carbon dioxide [8–11].

Introduction of transition metal ions (Me<sup>2+</sup>) to the zeolite matrix led to formation of several types of counter Me ion/oxo species: bare cations coordinated to oxygen atoms of the framework, cation-oxo species, bi(poly) nuclear cation-oxo species, metal (ion (oxo)) clusters and metal oxide species. Formation of these species depends on the zeolite topology, distribution of Al atoms in the zeolite matrix, metal loading and preparation procedure. Mostly, bare cations in extraframework cationic positions ( $\alpha$ -,  $\beta$ - and  $\gamma$ -sites) were proposed as the active sites for redox reaction [12, 13]. Depending on the conditions of catalyzed reaction, isolated cation-oxo species, bi(poly)nuclear cation-oxo species, metal (ion (oxo)) clusters and metal oxide species can perform redox catalytic cycles [9–11, 14, 15]. Recently, the highly effective active sites with two bare cooperating Fe cations in  $\beta$  cationic sites in ferrierite (FER) for N<sub>2</sub>O decomposition were proposed [12, 13, 16–18]. In recent years, significant developments have occurred in the field of the characterization of solids, connected predominantly with synchrotron-based methods as e.g. EXAFS/XANES and related methods, high-resolution XRD methods and X-ray tomography. However, the classic approach based on FTIR spectroscopy still shows significant potential in the study of bare cations in zeolites [19, 20]. Based on the FTIR spectroscopy results, cations can be analyzed using the perturbation of the antisymmetric T–O–T vibrations of the zeolite framework by the presence of bare cations (960–880 cm<sup>-1</sup>) or adsorption of the weak base d<sub>3</sub>-acetonitrile as a probe of Me<sup>2+</sup>. This contribution will focus on the employment of the T–O–T vibrations for characterization of the bare cations in ferrierite. The bonding of the cation (with preferred Me<sup>2+</sup>–O<sub>FRAMEWORK</sub> distance) in the cationic site results in the perturbation of the T–O–T angle of only a limited number of T–O–T framework structures adjacent to a metal ion [21–24].

The cation-specific FTIR spectra in the region of T–O–T vibrations have already been identified for mono-, di- and trivalent cations embedded in various zeolite matrices [14, 19, 21, 22, 25–28]. The positions of the band characterized bare cations located in  $\alpha$ ,  $\beta$  and  $\gamma$  positions in zeolites are site-specific and thus provide a unique and independent method to evaluate the respective occupation of the cation positions. It was shown that the intensities of the individual T–O–T bands increased linearly with the cation concentration and thus enabled semiquantitative evaluation of the cations anchored to the zeolite framework. The detailed analysis of the T–O–T region could also provide information on the formation of complexes between the cation and the external ligand, i.e. NO or NH<sub>3</sub> [21, 22]. The formation of a ligand–cation complex can be reflected in a shift of the T–O–T bands to higher wavenumbers [22, 29–32]. This finding represents an obstacle for the quantitative analysis of the bare cations in zeolites because the bands corresponding to bare Me<sup>2+</sup> cations and ligand–Me<sup>2+</sup> complexes could overlap. Moreover, cationic species that were not visible by FTIR spectroscopy were recently reported [15, 28, 33–35]. However, characterization of well-defined bare cations in the region of T–O–T vibrations by FTIR spectroscopy could offer a good basis for studying cations' behavior under redox conditions.

In this paper, a revision of the quantitative analysis of the siting of Co<sup>2+</sup> in the ferrierite matrix, with an emphasis of the possible presence of other than bare Co<sup>2+</sup> in the Co–zeolites, is made. The results for Co–ferrierite then serve as the comparison for the quantitative analysis of Mn<sup>2+</sup> and Ni<sup>2+</sup> in ferrierite. Particular attention is paid to the siting and distribution of bare Me<sup>2+</sup> in the ferrierites with a maximum loading of Me<sup>2+</sup> as crucial for the formation of binuclear Me<sup>2+</sup> cationic structures unique for ferrierite and suggested as highly active sites in redox reactions.

## Experimental

Commercially supplied ferrierite Si/Al 8.5 (Tosoh Corporation, Japan) was exchanged (3 × 24 h at room temperature (RT), 100 ml of a solution per 1 g of the zeolite) with either 1 M NaNO<sub>3</sub> or 1 M NH<sub>4</sub>NO<sub>3</sub>, washed

with distilled water and dried at ambient temperature.  $\text{NH}_4$ -FER and Na-FER were further exchanged to obtain  $\text{Co}^{2+}$ ,  $\text{Ni}^{2+}$  and  $\text{Mn}^{2+}$  forms of ferrierite with various metal loadings (Table 1). For the impregnation method,  $\text{NH}_4$ -FER was exclusively used as the starting material. Co-FER were prepared by ion exchange with 0.025–0.1 M solution of  $\text{Co}(\text{NO}_3)_2 \cdot 6\text{H}_2\text{O}$  at RT (for details, see Table 1). Mn-FER and Ni-FER were prepared by ion exchange using 0.005–0.33 M  $\text{Mn}(\text{NO}_3)_2 \cdot 4\text{H}_2\text{O}$  or  $\text{Ni}(\text{NO}_3)_2 \cdot 6\text{H}_2\text{O}$  at RT at 60 °C or 80 °C (Table 1). After the ion exchange, the zeolites were thoroughly washed with distilled water and dried in air at RT.

To obtain higher content of  $\text{Ni}^{2+}$  and  $\text{Mn}^{2+}$  in ferrierite, a dry impregnation method was used [36]. Parent  $\text{NH}_4$ - and H-FER were granulated to obtain a fraction of 0.3–0.6 mm grains and dehydrated at 120 °C for 4 h. The corresponding amount of  $\text{Mn}(\text{NO}_3)_2 \cdot 4\text{H}_2\text{O}$  or  $\text{Ni}(\text{NO}_3)_2 \cdot 6\text{H}_2\text{O}$  was dissolved in water and added dropwise to the zeolite to obtain  $\text{Ni}^{2+}$  and  $\text{Mn}^{2+}$  loading ranging from 0.5 to 2.0 wt%. Prepared samples were dried in static air for 24 h at RT. Then, zeolites were calcined in air at 450 °C for 4 h. The color change from light gray to dark gray was observed. The results of the elemental analysis of metal-containing zeolites carried out using X-ray fluorescence (XRF) are collected in Table 1.

FTIR spectra of the samples were collected on a Nicolet 6700 spectrometer equipped with a liquid nitrogen cooled detector with a resolution of  $2\text{ cm}^{-1}$ . The samples were prepared as self-supporting pellets ( $10\text{ mg/cm}^2$ ). Prior to the measurement, samples were evacuated under dynamic vacuum ( $10^{-3}\text{ Pa}$ ) at 450 °C (temperature ramp  $4\text{ °C/min}$ ) for 3 h. The Origin 8.1 software (OriginLab, Northampton, MA, USA) was used for data processing. FTIR spectra were simulated using previously established parameters characterizing cations in zeolites [14, 22, 32, 37].

**Table 1:** Chemical compositions of Co-, Ni- and Mn-ferrierites and conditions of their preparation.

	Chemical composition		Parameters of ion exchange			
	Me/Al	Me mmol/g	Solution	mol/l	Time h/repetition	Temperature K
Co $\text{NH}_4$ -FER	0.05	0.08	$\text{Co}(\text{NO}_3)_2$	0.025	6	298
	0.08	0.13	$\text{Co}(\text{NO}_3)_2$	0.025	12	298
	0.09	0.15	$\text{Co}(\text{NO}_3)_2$	0.050	16	298
	0.10	0.17	$\text{Co}(\text{NO}_3)_2$	0.050	24	298
	0.13	0.22	$\text{Co}(\text{NO}_3)_2$	0.050	$24 \times 2$	298
	0.18	0.30	$\text{Co}(\text{NO}_3)_2$	0.050	$24 \times 3$	298
	0.23	0.39	$\text{Co}(\text{NO}_3)_2$	0.050	$24 \times 3$	298
	0.25 <sup>a</sup>	0.42	$\text{Co}(\text{NO}_3)_2$	0.050	$24 \times 3$	298
	0.40 <sup>a</sup>	0.67	$\text{Co}(\text{acet})_2$	0.100	$5 \times 10$	343
Ni $\text{NH}_4$ -FER	0.04	0.07	$\text{Ni}(\text{NO}_3)_2$	0.050	24	333
	0.06	0.11	$\text{Ni}(\text{NO}_3)_2$	0.150	$24 \times 3$	333
	0.07	0.12	$\text{Ni}(\text{NO}_3)_2$	0.100	$24 \times 3$	333
	0.08	0.13	$\text{Ni}(\text{NO}_3)_2$	0.100	$24 \times 3$	333
NiNa-FER	0.17	0.29	$\text{Ni}(\text{NO}_3)_2$	0.050	$24 \times 3$	353
NiH-FER	0.29	0.49	$\text{Ni}(\text{NO}_3)_2$	0.610	Impregnation	298
	0.36	0.60	$\text{Ni}(\text{NO}_3)_2$	0.680	Impregnation	298
Mn $\text{NH}_4$ -FER	0.05	0.08	$\text{Mn}(\text{NO}_3)_2$	0.005	12	298
	0.06	0.11	$\text{Mn}(\text{NO}_3)_2$	0.005	24	298
	0.10	0.17	$\text{Mn}(\text{NO}_3)_2$	0.025	24	298
	0.12	0.20	$\text{Mn}(\text{NO}_3)_2$	0.010	$24 \times 3$	298
	0.16	0.27	$\text{Mn}(\text{NO}_3)_2$	0.080	$24 \times 3$	298
	0.21	0.35	$\text{Mn}(\text{NO}_3)_2$	0.100	$24 \times 3$	353
MnNa-FER	0.32	0.54	$\text{Mn}(\text{NO}_3)_2$	0.080	$24 \times 3$	298
MnH-FER	0.38	0.59	$\text{Mn}(\text{NO}_3)_2$	0.560	Impregnation	298

<sup>a</sup>Data from [37].

## Me<sup>2+</sup> (Co<sup>2+</sup>, Mn<sup>2+</sup> and Ni<sup>2+</sup>) siting in ferrierite

The effect of the binding of countercation in the dehydrated zeolites on the FTIR spectra of antisymmetric T–O–T vibrations of the zeolite framework (980–880 cm<sup>-1</sup>) is depicted in Fig. 1. The FTIR spectrum of the H–FER in the region of T–O–T vibrations did not exhibit any bands. The coordination of cations to the Al atoms in the ferrierite ring results in the perturbation of T–O–T vibrations, which is reflected in the formation of new complex bands between 980 and 880 cm<sup>-1</sup> (see Figs. 1 and 2). Simulations of the spectra provided the following T–O–T bands: 942, 918 and 885 cm<sup>-1</sup> for Co–ferrierite, 940, 918 and 879 cm<sup>-1</sup> for Ni–ferrierite and 953, 928 and 902 cm<sup>-1</sup> for Mn–ferrierite. The latter bands are observed only at the highest Me<sup>2+</sup> loadings. The position of the first two bands for Co– and Mn–ferrierites fits those already reported, while those for Ni–ferrierite only slightly differ as is shown in Table 2 [22]. The wavenumber corresponding to the third band for Ni–ferrierite and Mn–ferrierite was not reported before, while the value obtained for Co–ferrierite is in agreement with previous findings [29, 30].

However, these bands were attributed to the shifted antisymmetric T–O–T stretching vibrations of the zeolitic lattice induced by binding of bare Me<sup>2+</sup> in cationic positions, the shift of the T–O–T vibrations to higher wavenumbers due to the weakening of the ligation of the cation to the framework by the formation

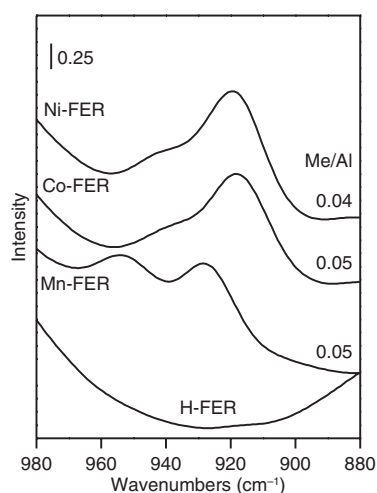


Fig. 1: FTIR spectra of perturbed T–O–T antisymmetric mode of dehydrated H–, MnH–, CoH– and NiH–FER samples.

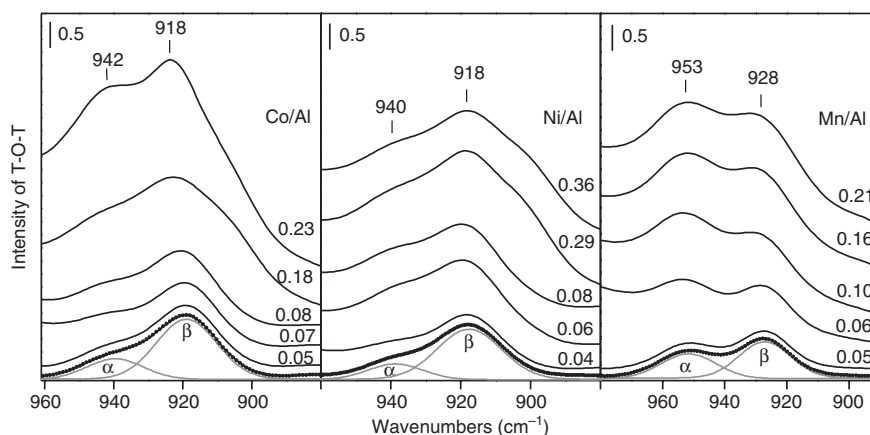


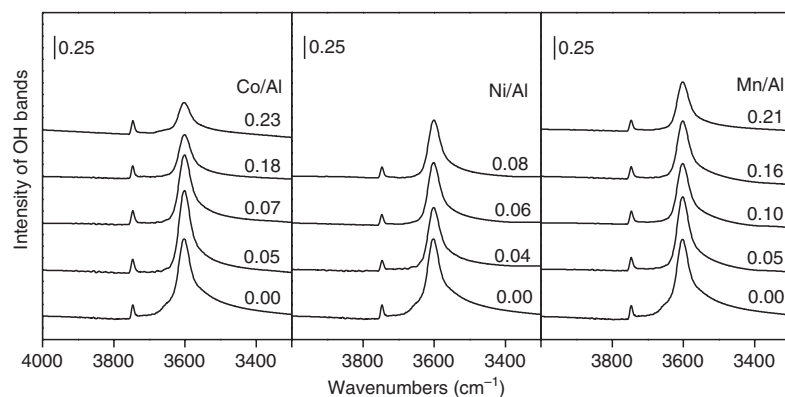
Fig. 2: FTIR spectra of perturbed T–O–T antisymmetric mode of dehydrated CoH–FER, NiH–FER and MnH–FER samples with various metal loadings (Me/Al) and simulations of selected spectra as Gaussian bands.

**Table 2:** Wavenumbers of T–O–T vibrations reflecting cations in the  $\alpha$ -,  $\beta$ - and  $\gamma$ -sites for Co-, Ni- and Mn-ferrierites, numbers in brackets are taken from Ref. [20].

	$\alpha$	$\beta$	$\gamma$	Extinction coefficient
	cm <sup>-1</sup>			cm $\mu$ mol <sup>-1</sup>
Mn	953 (953)	928 (927)	902	30.4
Co	942 (943)	918 (917)	885	38.5
Ni	940 (943)	918 (913)	879	35.8

of the Me<sup>2+</sup>-ligand complex was reported [22]. Thus, FTIR spectra of bare Me<sup>2+</sup>-ferrierites in the region of OH vibrations (see Fig. 3) were analyzed and confirmed the presence of bands exclusively attributed to skeletal OH groups. A narrow band at 3747 cm<sup>-1</sup> reflects terminal silanol groups (Si–OH) with weak acidity [38–40]. The narrow band at 3601 cm<sup>-1</sup> corresponds to the unperturbed and a broad low-intensity absorption between 3600 and 3350 cm<sup>-1</sup> to the perturbed framework Brønsted bridging groups (Al–OH–Si) [38–40]. No band between 3600 and 3700 cm<sup>-1</sup> attributable to the Me<sup>2+</sup>–OH complexes [38–41] was present in the spectra of Me<sup>2+</sup>-zeolites with Me<sup>2+</sup> loadings below the maximum, see Fig. 3. Nevertheless, besides well-known Me<sup>2+</sup>–OH species balancing only one framework Al atom, also monovalent [Me<sup>3+</sup>O<sup>2-</sup>]<sup>+</sup> complexes were recently suggested to be possibly formed in zeolites; [Co<sup>3+</sup>O<sup>2-</sup>]<sup>+</sup> complexes were reported for Co-beta and Co-SSZ-13 zeolites [28, 33, 34]. These monovalent species are not reflected in the FTIR or UV-vis spectra. Thus, the only way for the unambiguous analysis of monovalent and divalent Me<sup>2+</sup> species in dehydrated zeolite is a quantitative study of Brønsted bridging groups (terminal Si–OH groups of weak acidity that are unable to accommodate cations). This analysis is concluded in Fig. 4. At least up to Me/Al = 0.15, two Brønsted Si–OH–Al groups are consumed for the accommodation of one Me<sup>2+</sup>. This clearly demonstrated that below this metal ion loading, exclusively  $\beta$  bare Me<sup>2+</sup> cations in  $\alpha$  and are present in the zeolite. The deviation from this ratio at higher metal loadings (Me/Al > 0.15) indicates that other species than bare divalent cations should be present in highly metal-loaded samples. In Co-ferrierite with highest Co loading, Co/Al 0.40, 78 % of introduced cations should correspond to monovalent species (this is the upper limit because also uncharged Co-oxo species should be formed), for maximum exchanged Mn-ferrierite (Mn/Al 0.21) 70 %. These results confirmed that analysis of coordination of the cation in the vicinity of one or two Al atoms is essential for the investigation of cation siting and distribution in the zeolite [15].

The above results indicate that both low- and medium-loaded ferrierite (Me/Al < 0.25) exhibited a band in the FTIR spectrum in the region of perturbed T–O–T vibrations reflecting the siting of bare Me<sup>2+</sup>. Thus, the bands at 942, 918 and 885 cm<sup>-1</sup> of Co-ferrierite, 940, 918 and 879 cm<sup>-1</sup> of Ni-ferrierite and 953, 928 and 902 cm<sup>-1</sup> of Mn-ferrierite reflect bare Me<sup>2+</sup> located in  $\alpha$ -,  $\beta$ - and  $\gamma$ -sites of the ferrierite framework, were assigned to

**Fig. 3:** FTIR spectra of the region of OH vibrations of Co-FER, Ni-FER and Mn-FER with various metal loadings (Me/Al).

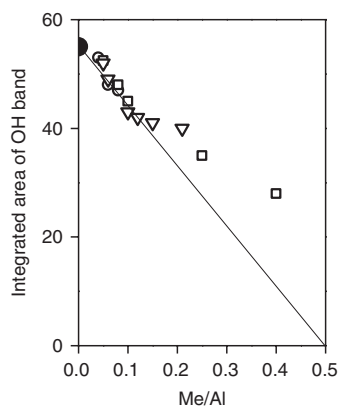


**Fig. 4:** Effect of metal loading (Me/Al) on the intensities of Brønsted acid sites of Co-FER (□), Ni-FER (○) and Mn-FER (▽) and intensity of Brønsted acid sites of parent H-FER (●). The line indicates the replacement of two protons by one divalent cation.

respective cation positions. Note that previous studies did not exclude the formation of monovalent cationic complexes. Using *ab initio* calculations, the location of cationic sites and the local arrangement of cationic  $\alpha$ - and  $\beta$ -sites were already predicted (Fig. 5) [13, 29, 30, 37, 42–45]. In contrast to the cations in the  $\alpha$ - and  $\beta$ -sites, the detailed structure of the  $\gamma$ -site cannot be suggested due to the unknown location of Al atoms in this site ( $\alpha$ -site is formed by two Al atoms, the T1, and  $\beta$ -site by two Al in the T2 sites) [46]. The suggested attribution of cationic sites to the T–O–T band is further confirmed by the analysis of cation siting in highly loaded zeolites. In this case, cation siting is directly controlled by the distribution of Al atoms (2 Al atoms in one six-membered ring) in individual cationic sites. This point will be discussed in the subsequent section.

## Quantitative analysis of $\text{Me}^{2+}$ ( $\text{Co}^{2+}$ , $\text{Mn}^{2+}$ and $\text{Ni}^{2+}$ ) siting in ferrierite

The exclusive presence of bare cations in samples with  $\text{Me}/\text{Al} < 0.15$  allows estimation of extinction coefficients of cations in individual cationic sites serving for the quantitative analysis of  $\text{Me}^{2+}$  siting in the zeolite. The effect of metal loading on the intensity of the T–O–T vibration for Me-ferrierites is depicted in Fig. 6. For  $\text{Me}/\text{Al} < 0.15$ , there is a linear dependence of the intensity of T–O–T vibrations on the metal loading although several spectral components reflect siting of  $\text{Me}^{2+}$  in the  $\alpha$ - and  $\beta$ -sites. This suggests that extinction coefficients of  $\text{Me}^{2+}$  in the  $\alpha$ - and  $\beta$ -sites are similar, although the geometry of the sites and cation coordinations are different [13, 44, 47]. However, the variability of the occupation of cationic sites in samples with low metal loading is rather low as follows from Fig. 7. Cations for the Me-FER with low metal loading ( $\text{Me}/\text{Al}$  0.15) predominantly occupied  $\alpha$  and  $\beta$  cationic sites (see Fig. 7). It was calculated on the basis on the experimental

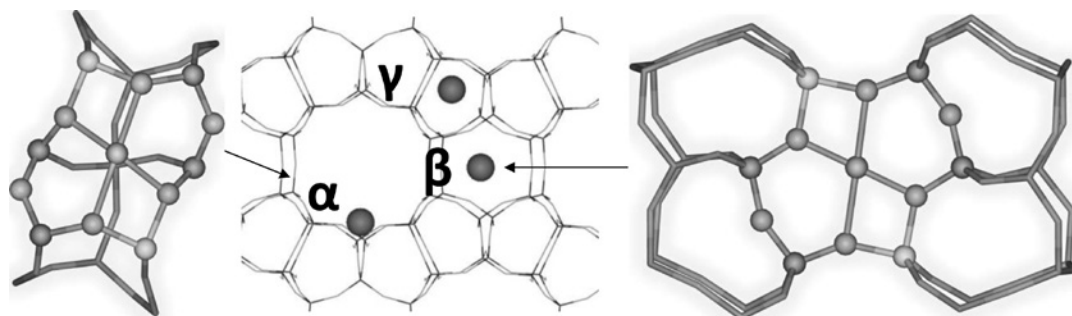


**Fig. 5:** Location of  $\text{Me}^{2+}$  cations in  $\alpha$ -,  $\beta$ - and  $\gamma$ -sites in the ferrierite structure and optimized structures of the  $\alpha$ - and  $\beta$ -sites of  $\text{Me}^{2+}$ -ferrierite after molecular dynamics simulations according to Refs. [13, 43, 44, 46].

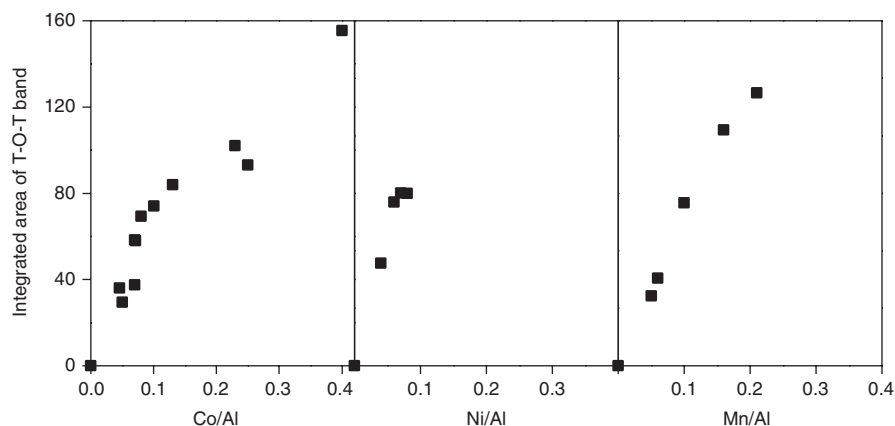


**Fig. 6:** Effect of Me loading in Co-FER, Ni-FER and Mn-FER on the integrated intensity of the T–O–T vibrations perturbed by the accommodated  $\text{Me}^{2+}$  ( $980\text{--}880\text{ cm}^{-1}$ ).

data, Figs. 6 and 7, that differences in extinction coefficient values up to 25 % caused observable change on the level of 5 % in linear dependence of T–O–T vibrations.

Nevertheless, the recent analysis of the Co siting in the zeolite SSZ-13 [28] demonstrated the changes in the occupation of individual sites while the total intensity of perturbed T–O–T vibrations was linear with the content of bare  $\text{Co}^{2+}$ . It can be suggested that the extinction coefficients of  $\text{Me}^{2+}$  located in different cationic sites of ferrierite are the same within experimental error. The extinction coefficients obtained from the linear regression of the concentration dependence of the intensity of T–O–T vibration on metal loading in the concentration region below  $\text{Me}/\text{Al} = 0.15$  are presented in Table 2. However, while similar extinction coefficients were suggested for the cation in different sites, Table 2 shows significant differences between the extinction coefficients of different cations (up to 25 %). Without an explanation of this discrepancy, quantitative analysis of the concentration of bare  $\text{Me}^{2+}$  via perturbed T–O–T vibrations is unacceptable. The arrangement of occupied cationic sites represents the result of the interplay between the cation inducing the deformation, coordination and flexibility of the empty cationic site in zeolites. Although the arrangement of cationic sites differs, there is no reason to expect different capability of the cation to perturb the cationic site, which was suggested to be its intrinsic property (e.g. hydration heat or hydration diameter was suggested) [22, 23]. Thus, the arrangements of cationic sites with the cation can be suggested to be a result of similar “strength” of the perturbation (cation specific) on different starting rings.

The exact relationship between the perturbation of T–O–T vibration and corresponding T–O–T wave-number is not known, however, their correlation (evidenced by the similar changes of T–O–T bands with the

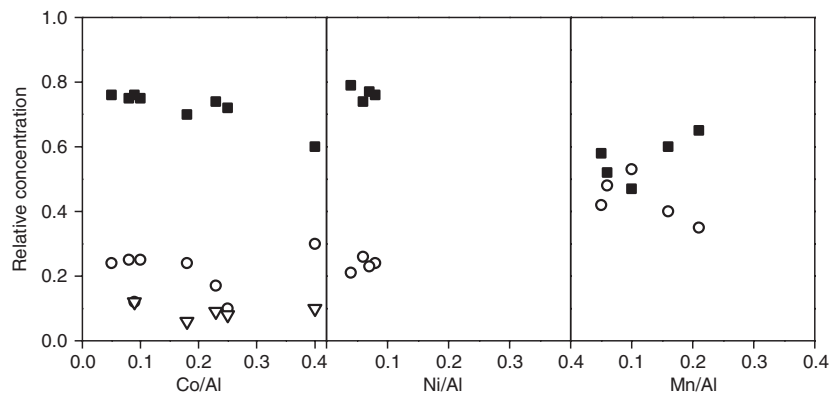


**Fig. 7:** Dependence of the relative concentration of the  $\alpha$ - (O),  $\beta$ - (■) and  $\gamma$ -sites (▽) of  $\text{Co}^{2+}$ ,  $\text{Ni}^{2+}$  and  $\text{Mn}^{2+}$  on the ratio of  $\text{Me}/\text{Al}$  in ferrierite.

cation) can be discussed. The observed differences in wavenumbers of perturbed T–O–T vibrations of  $\alpha$ -,  $\beta$ - or  $\gamma$ -sites represent differences in the parent T–O–T vibrations of empty sites, thus the shift of vibrations due to the perturbation caused by cations can be suggested as similar. This assumption permits explaining the rather low effect of cation (Co, Mn or Ni) on the position of bands of individual cationic sites, which changed by less than  $14\text{ cm}^{-1}$ . In contrast, the differences in the position of the most intense bands  $\alpha$  and  $\beta$  for particular cations differs by more than  $22\text{ cm}^{-1}$  (e.g. for Co–ferrierite:  $\alpha\ 942\text{ cm}^{-1}$  and  $\beta\ 918\text{ cm}^{-1}$ ). The changes in the positions of the bands of  $\alpha$ - and  $\beta$ -sites for Co, Ni or Mn do not influence significantly the perturbations of the T–O–T vibrations. This suggests that the value of extinction coefficients for the cation at different cationic sites should be similar. The abovementioned differences of extinction coefficients of different cations clearly demonstrated that they can be employed only for the analysis of the siting of the given cation.

## Speciation of $\text{Me}^{2+}$ ( $\text{Co}^{2+}$ , $\text{Mn}^{2+}$ and $\text{Ni}^{2+}$ ) in ferrierite

It is well known that besides bare  $\text{Me}^{2+}$  cations, other cationic species could be introduced to the zeolites. The type of the present cationic species in dehydrated zeolites is the result of two complex processes – metal ion introduction and zeolite dehydration/activation. Only in the case of the exclusive presence of bare  $\text{Me}^{2+}$  cations in the zeolite and occupation of all cationic sites for divalent cations, the concentration of bare  $\text{Me}^{2+}$  cations and their distribution in individual sites ( $\alpha$ ,  $\beta$  and  $\gamma$ ) is given by the Al distribution in the zeolite framework. As was previously proved, only Al pairs (two Al atoms in 6- or 8-membered rings of ferrierite) in cationic positions ( $\alpha$ ,  $\beta$  or  $\gamma$ ) stabilized bare  $\text{Me}^{2+}$ . In the investigated ferrierite matrix, 62% of Al atoms are located as Al pairs [15, 18, 38, 39]. Approximately 70% of Al pairs are situated in the  $\beta$ -site and 20% in the  $\alpha$ -site [37, 46]. Cations located in both  $\beta$  and  $\alpha$  cationic sites are suggested as active sites for redox processes due to their facility in the changes of oxidation state and the open coordination sphere (structure published [13, 45, 47]).

Figure 8 depicts the concentration of bare  $\text{Me}^{2+}$  ( $\text{Me}/\text{Al}$ ) and their location in  $\beta$ -,  $\alpha$ - and  $\gamma$ -sites in dehydrated MeH–ferrierites prepared using the ion exchange method. For all concentration ranges,  $\text{Co}^{2+}$  and  $\text{Ni}^{2+}$  in ferrierite are predominantly located in the  $\beta$ -site while the concentrations of  $\text{Mn}^{2+}$  in the  $\alpha$ - and  $\beta$ -sites of ferrierite are comparable. This indicates a higher stabilization energy for  $\text{Co}^{2+}$  and  $\text{Ni}^{2+}$  in the  $\beta$ -site than in the  $\alpha$ -site. The  $\alpha$ -site in ferrierite is easily accessible through the main 10-member ring channel while access to

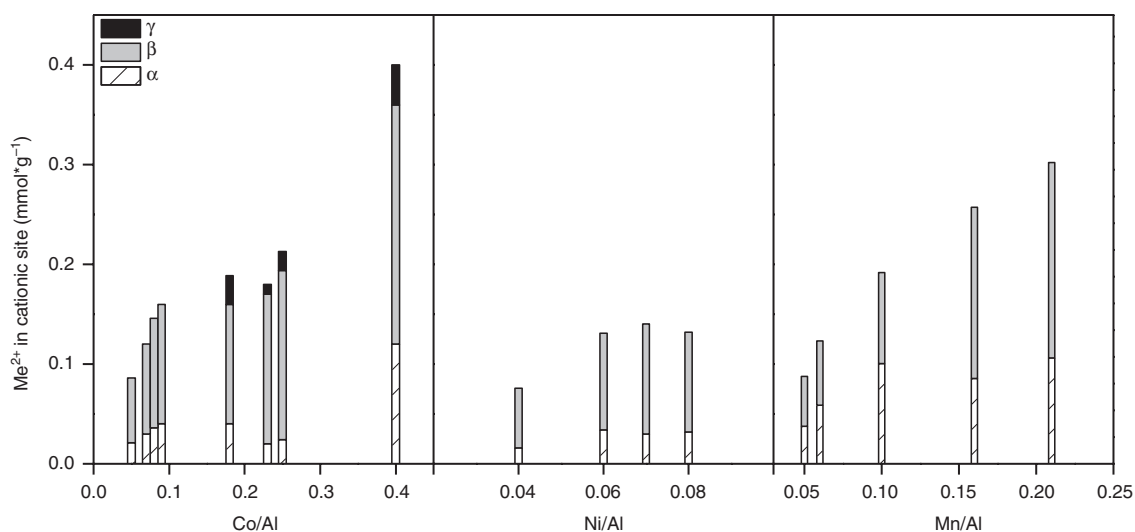


**Fig. 8:** The concentration of bare  $\text{Me}^{2+}$  and their distribution in  $\alpha$ -,  $\beta$ - and  $\gamma$ -sites in dehydrated MeH–ferrierites prepared by ion exchange.

the  $\beta$ -site is limited by the 8-membered ring. Bare  $\text{Me}^{2+}$  in  $\alpha$ - and  $\beta$ -sites of ferrierite are exclusively present in  $\text{Me}/\text{Al} < 0.15$  (Fig. 6). However, for  $\text{Ni}^{2+}$  and  $\text{Mn}^{2+}$ , the maximum concentration of bare  $\text{Me}^{2+}$  prepared using the ion exchange method is rather low (maximum  $\text{Me}/\text{Al}$  values are 0.09 for  $\text{NiH}$ - and 0.21 for  $\text{MnH}$ -ferrierites). The analysis of the distribution of Al atoms in studied ferrierites revealed that the limit for bare divalent cations is  $\text{Me}/\text{Al}$  0.31 [37]. Among studied  $\text{Me}$ -ferrierites prepared by ion exchange, only  $\text{CoNH}_4$ -ferrierite provides a highly loaded sample ( $\text{Co}/\text{Al}$  0.40). However, this ion exchange degree is above the maximum ion exchange capacity of the parent ferrierite for bare  $\text{Me}^{2+}$  (see above), thus the formation of other species than bare  $\text{Me}^{2+}$  is expected.

To reach higher concentrations of bare cations in the ferrierite, two different preparation methods for Ni and Mn cations were applied: (i) ion exchange to the  $\text{Na}$ -ferrierite and (ii) impregnation of the  $\text{NH}_4$ -ferrierite. While ion exchange of the  $\text{Na}$  form of parent ferrierite allows to reach maximum ion exchange capacity for divalent cation for  $\text{Co}^{2+}$  (0.32) [37] and  $\text{Mn}^{2+}$  ( $\text{Me}^{2+}/\text{Al}$  0.32), the ion exchange degree for  $\text{Ni}^{2+}$  is still low ( $\text{Ni}/\text{Al}$  0.17). The high Ni loading ( $\text{Ni}/\text{Al}$  0.29 and 0.36) in ferrierite was reached by impregnation of parent ferrierite by  $\text{Ni}(\text{NO}_3)_2$ . Analogously, in the case of  $\text{Mn}$ -ferrierite, impregnation resulted in high manganese loading in ferrierite,  $\text{Mn}/\text{Al}$  0.38. The FTIR spectra of nickel and manganese ferrierite with high metal loading prepared using the impregnation method are presented in Fig. 9. The concentration of bare  $\text{Me}^{2+}$  cations and their distribution between individual cationic sites for maximum exchanged  $\text{Me}$ -ferrierites are given in Fig. 10.

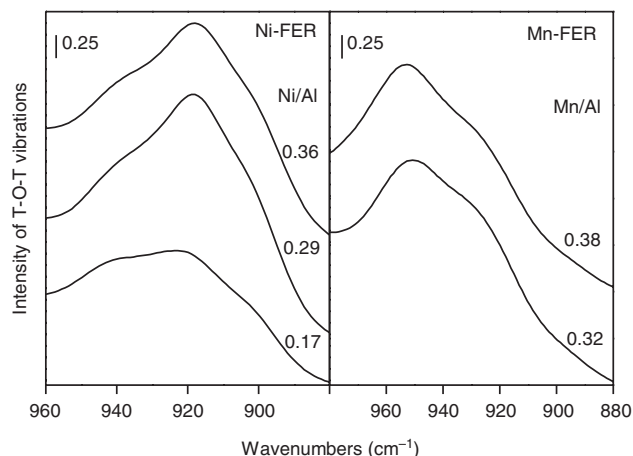


**Fig. 9:** FTIR spectra of the perturbed T–O–T antisymmetric mode of NiNa–FER ( $\text{Ni}/\text{Al}$  0.17) and impregnated NiH–FER ( $\text{Ni}/\text{Al}$  0.29 and 0.36), MnNa–FER ( $\text{Mn}/\text{Al}$  0.32) and impregnated MnH–FER ( $\text{Mn}/\text{Al}$  0.38).

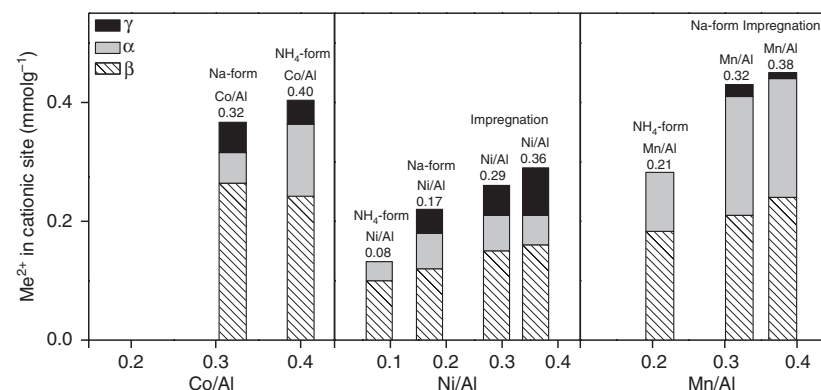


**Fig. 10:** The concentration of bare  $\text{Me}^{2+}$  and their distribution in  $\alpha$ -,  $\beta$ - and  $\gamma$ -sites in dehydrated maximum loaded  $\text{MeH}$ - and  $\text{MeNa}$ -ferrierites prepared by ion exchange and  $\text{MeH}$ -ferrierite prepared by impregnation. Data for  $\text{Co}/\text{Al}$  0.32 taken from Ref. [37].

The ion exchange of  $\text{Co}^{2+}$  to the NaK-ferrierite results in maximum possible loading of bare  $\text{Co}^{2+}$  ( $\text{Co}_{\text{BARE}}/\text{Al}$  0.32), exclusively [37]. Thus, ion exchange from both  $\text{NH}_4$ -ferrierite and Na-ferrierite represents a simple but powerful method for the preparation of Co-ferrierites with bare  $\text{Co}^{2+}$ . Location of Co cations in cationic sites in both maximum exchanged samples (Co/Al 0.31), which is controlled by the distribution of Al atoms in ferrierite, confirmed that 70–75 % of  $\text{Co}^{2+}$  is present in the  $\beta$ -site, 15–20 % is located in the  $\alpha$ -site and 10 % of  $\text{Co}^{2+}$  is accommodated in the  $\gamma$ -site [37]. Ion exchange of  $\text{Ni}^{2+}$  to the  $\text{NH}_4$ - and Na-ferrierite (Ni/Al 0.08 and 0.17, respectively) provides the exclusive presence of bare  $\text{Ni}^{2+}$  with the prevailing location of  $\text{Ni}^{2+}$  in the  $\beta$ -site. Nevertheless, the total amount of bare  $\text{Ni}^{2+}$  is rather low ( $\text{Ni}_{\text{BARE}}/\text{Al}$  0.17 for the ion exchange method from Na-ferrierite). The introduction of  $\text{Ni}^{2+}$  to the  $\text{NH}_4$ -ferrierite by impregnation provides significantly higher Ni loading in the sample (Ni/Al 0.36), but still less than 60 % of Ni cations were present in the form of bare  $\text{Ni}^{2+}$  ( $\text{Ni}_{\text{BARE}}/\text{Al}$  0.20). Among them, 60 % of  $\text{Ni}^{2+}$  are located in the  $\beta$ -site, 15 % in the  $\alpha$ -site and 25 % in the  $\gamma$ -site. It indicates that the impregnation method leads to the increasing presence of  $\text{Ni}^{2+}$  in the  $\gamma$ -site. It was shown that the cations in the  $\gamma$ -site with pseudo-octahedral coordination and closed coordination sphere [37, 42, 43] are protected against transformation to oxo species and formed in the overexchanged samples. Ion exchange of  $\text{Mn}^{2+}$  to the Na-ferrierite, as well as impregnation, provides highly loaded samples with Mn/Al 0.32 and 0.38, respectively. Both samples contain a high amount of bare  $\text{Mn}^{2+}$  (Mn/Al 0.32 and 0.38), however, Mn-ferrierite prepared using the impregnation method shows that ca 20 % of Mn species is present in a form other than bare  $\text{Mn}^{2+}$ .

The above results show that Co-, Mn- and Ni-ferrierites with predominantly bare cations can be prepared not only for low Me loaded samples but also for samples with the maximum occupation of cationic sites for bare divalent cations. Such samples contain the maximum concentration of bare  $\text{Me}^{2+}$  – the most frequent type of catalytic centers in the reactions catalyzed by metallozeolites. Moreover, these highly loaded with bare  $\text{Me}^{2+}$  samples guarantee the formation of the unique type of the active site exclusively connected with the ferrierite topology – the pair of cooperating bare  $\text{Me}^{2+}$  [13, 47]. In the case of  $\text{Co}^{2+}$  and  $\text{Mn}^{2+}$ , the ion exchange procedure provides samples highly loaded with bare  $\text{Me}^{2+}$  located opposite to each other. In the case of  $\text{Ni}^{2+}$ , ion exchange does not result in high enough incorporation of the metal ions to the zeolite and the impregnation procedure has to be employed.

## Conclusions

FTIR spectroscopy of perturbed antisymmetric T–O–T vibrations represents a powerful tool for the (semi) quantitative analysis of the bare  $\text{Me}^{2+}$ , their siting and distribution in the dehydrated metallozeolites, as was demonstrated for the ferrierite matrix. Nevertheless, proper estimation of extinction coefficients allowing this analysis requires a combination of the FTIR spectroscopy of T–O–T vibrations with a supplementary method for the analysis of residual cations in parent zeolite. This can be done in the case of  $\text{NH}_4$ -zeolites by the quantitative analysis of residual Brønsted bridging Al–OH–Si sites. Only samples with exclusive presence of bare  $\text{Me}^{2+}$  (i.e. ions replacing two Brønsted acid sites) can be employed for the estimation of the extinction coefficients of bare  $\text{Me}^{2+}$ .

Extinction coefficients for bare  $\text{Ni}^{2+}$  and  $\text{Mn}^{2+}$  located in the ferrierite zeolite matrix were established and the coefficient for  $\text{Co}^{2+}$  was examined and they were employed for the quantitative analysis of  $\text{Me}^{2+}$  speciation in ferrierite.

$\text{Co}^{2+}$ ,  $\text{Ni}^{2+}$  and  $\text{Mn}^{2+}$  occupy previously reported  $\alpha$ -,  $\beta$ - and  $\gamma$ -sites for extraframework cations in the ferrierite matrix. Wavenumbers of antisymmetric T–O–T vibrations reflecting  $\text{Co}^{2+}$ ,  $\text{Ni}^{2+}$  and  $\text{Mn}^{2+}$  in the  $\alpha$ - and  $\beta$ -sites were confirmed, while they were estimated for cations  $\text{Ni}^{2+}$  and  $\text{Mn}^{2+}$  in the  $\gamma$ -sites. It was proven and explained that the extinction coefficients of the cations in individual sites exhibited similar values and can be taken for quantitative analysis.

Co-, Ni- and Mn-ferrierites with maximum possible loading of bare  $\text{Co}^{2+}$ ,  $\text{Ni}^{2+}$  and  $\text{Mn}^{2+}$  in cationic sites were successfully prepared by the ion exchange or impregnation methods. Such samples guarantee not only

a high concentration of bare  $\text{Me}^{2+}$  as active sites in ferrierite catalysts but also the formation of specific types of ferrierite active sites—pairs of bare  $\text{Me}^{2+}$ .

**Acknowledgments:** This work was supported by the Grant Agency of the Czech Republic, Funder Id: <http://dx.doi.org/10.13039/501100001824>, under projects # 17-00742S and the RVO: 61388955. Chemical analyses of samples were provided in the frame of CATPRO (Ministry of Education, Youth and Sports, ref. no. MSMT-1000/2016, Funder Id: <http://dx.doi.org/10.13039/501100001823>, under Project No. LM2015039), which has been integrated into the National Program for Sustainability I of the Ministry of Education, Youth and Sports of the Czech Republic through the project Development of the UniCRE Centre, Project Code LO1606.

## References

- [1] R. M. Barrer. *Hydrothermal Chemistry of Zeolites*, Academic Press, London (1982).
- [2] J. Weitkamp, M. Hunger. in *Introduction to Zeolite Science and Practice*, J. Cejka, H. van Bekkum, A. Corma, F. Schuth (Eds.), p. 787 (2007).
- [3] H. van Bekkum, E. M. Flanigen, J. C. Jansen, (Eds.), *Introduction to Zeolite Science and Practice*, Elsevier, Amsterdam (1991).
- [4] A. Corma. *Chem. Rev.* **95**, 559 (1995).
- [5] A. Primo, H. Garcia. *Chem. Soc. Rev.* **43**, 7548 (2014).
- [6] A. M. Beale, F. Gao, I. Lezcano-Gonzalez, C. H. F. Peden, J. Szanyi. *Chem. Soc. Rev.* **44**, 7371 (2015).
- [7] P. Bhanja, A. Bhaumik. *Fuel* **185**, 432 (2016).
- [8] Z. Bian, S. Das, M. H. Wai, P. Hongmanorom, S. Kawi. *ChemPhysChem* **18**, 3117 (2017).
- [9] K. Narsimhan, K. Iyoki, K. Dinh, Y. Roman-Leshkov. *ACS Cent. Sci.* **2**, 424 (2016).
- [10] M. Ravi, M. Ranocchiari, J. A. van Bokhoven. *Angew. Chem. Int. Ed.* **56**, 16464 (2017).
- [11] Z. Zakaria, S. K. Kamarudin. *Renew. Sus. Eng. Rev.* **65**, 250 (2016).
- [12] J. Dedecek, L. Capek, P. Sazama, Z. Sobalik, B. Wichterlova. *Appl. Catal. A* **391**, 244 (2011).
- [13] S. Sklenak, P. C. Andrikopoulos, B. Boekfa, B. Jansang, J. Novakova, L. Benco, T. Bucko, J. Hafner, J. Dedecek, Z. Sobalik. *J. Catal.* **272**, 262 (2010).
- [14] Z. Sobalik, J. Dedecek, I. Ikonnikov, B. Wichterlova. *Microporous Mesoporous Mater.* **21**, 525 (1998).
- [15] J. Dedecek, Z. Sobalik, B. Wichterlova. *Catal. Rev. Sci. Eng.* **54**, 135 (2012).
- [16] Z. Sobalik, J. Novakova, J. Dedecek, N. K. Sathu, E. Tabor, P. Sazama, P. Stastny, B. Wichterlova. *Microporous Mesoporous Mater.* **146**, 172 (2011).
- [17] Z. Sobalik, P. Sazama, J. Dedecek, B. Wichterlova. *Appl. Catal. A* **474**, 178 (2014).
- [18] E. Tabor, K. Zaveta, N. K. Sathu, A. Vondrova, P. Sazama, Z. Sobalik. *Catal. Today* **175**, 238 (2011).
- [19] G. D. Lei, B. J. Adelman, J. Sarkany, W. M. H. Sachtler. *Appl. Catal. B* **5**, 245 (1995).
- [20] J. Sárkány. *J. Mol. Struct.* **410–411**, 95 (1997).
- [21] Z. Sobalik, Z. Tvaruzkova, B. Wichterlova. *Microporous Mesoporous Mater.* **25**, 225 (1998).
- [22] Z. Sobalik, Z. Tvaruzkova, B. Wichterlova. *J. Phys. Chem. B* **102**, 1077 (1998).
- [23] J. E. Sponer, Z. Sobalik, J. Leszczynski, B. Wichterlova. *J. Phys. Chem. B* **105**, 8285 (2001).
- [24] R. A. van Santen, D. L. Vogel. *Adv. Solid State Chem.* **1**, 1551 (1989).
- [25] W. Jacobs, J. Vanwolput, R. Vansanten. *Zeolites* **13**, 170 (1993).
- [26] J. H. Kwak, T. Varga, C. H. F. Peden, F. Gao, J. C. Hanson, J. Szanyi. *J. Catal.* **314**, 83 (2014).
- [27] R. Karcz, J. Dedecek, B. Supronowicz, H. M. Thomas, P. Klein, E. Tabor, P. Sazama, V. Pashkova, S. Sklenak. *Chem. Eur. J.* **23**, 8857 (2017).
- [28] K. Mlekodaj, J. Dedecek, V. Pashkova, E. Tabor, P. Klein, M. Urbanova, R. Karcz, P. Sazama, S. R. Whittleton, H. M. Thomas, A. V. Fishchuk, S. Sklenak. *J. Phys. Chem. C* **123**, 7968 (2019).
- [29] Z. Sobalik, J. Dedecek, D. Kaucky, B. Wichterlova, L. Drozdova, R. Prins. *J. Catal.* **194**, 330 (2000).
- [30] L. Drozdova, R. Prins, J. Dedecek, Z. Sobalik, B. Wichterlova. *J. Phys. Chem. B* **106**, 2240 (2002).
- [31] L. Capek, V. Kreibich, J. Dedecek, T. Grygar, B. Wichterlova, Z. Sobalik, J. A. Martens, R. Brosius, V. Tokarova. *Microporous Mesoporous Mater.* **80**, 279 (2005).
- [32] J. Dedecek, L. Capek, D. Kaucky, Z. Sobalik, B. Wichterlova. *J. Catal.* **211**, 198 (2002).
- [33] L. Capek, J. Dedecek, P. Sazama, B. Wichterlova. *J. Catal.* **272**, 44 (2010).
- [34] L. Capek, J. Dedecek, B. Wichterlova. *J. Catal.* **227**, 352 (2004).
- [35] P. Sazama, E. Tabor, P. Klein, B. Wichterlova, S. Sklenak, L. Mokrzycki, V. Pashkova, M. Ogura, J. Dedecek. *J. Catal.* **333**, 102 (2016).
- [36] D. P. Gamliel, B. P. Baillie, E. Augustine, J. Hall, G. M. Bollas, J. A. Valla. *Microporous Mesoporous Mater.* **261**, 18 (2018).

- [37] D. Kaucky, J. I. Dedecek, B. Wichterlova. *Microporous Mesoporous Mater.* **31**, 75 (1999).
- [38] E. Tabor, G. Sádovská, M. Bernauer, P. Sazama, J. Nováková, V. Fíla, T. Kmječ, J. Kohout, K. Závěta, Z. Sobalík. *Appl. Catal. B* **240**, 358 (2019).
- [39] E. Tabor, K. Jisa, J. Novakova, Z. Bastl, A. Vondrova, K. Zaveta, Z. Sobalik. *Microporous Mesoporous Mater.* **165**, 40 (2013).
- [40] G. Sádovská, E. Tabor, P. Sazama, M. Lhotka, M. Bernauer, Z. Sobalik. *Catal. Commun.* **89**, 133 (2017).
- [41] B. Wichterlova, Z. Tvaruzkova, Z. Sobalik, P. Sarv. *Microporous Mesoporous Mater.* **24**, 223 (1998).
- [42] M. C. Dalconi, A. Alberti, G. Cruciani, P. Ciambelli, E. Fonda. *Microporous Mesoporous Mater.* **62**, 191 (2003).
- [43] M. C. Dalconi, G. Cruciani, A. Alberti, P. Ciambelli, M. T. Rapacciuolo. *Microporous Mesoporous Mater.* **39**, 423 (2000).
- [44] L. Benco, T. Bucko, R. Grybos, J. Hafner, Z. Sobalik, J. Dedecek, S. Sklenak, J. Hrusak. *J. Phys. Chem. C* **111**, 9393 (2007).
- [45] S. Sklenak, P. C. Andrikopoulos, S. R. Whittleton, H. Jirglova, P. Sazama, L. Benco, T. Bucko, J. Hafner, Z. Sobalik. *J. Phys. Chem. C* **117**, 3958 (2013).
- [46] J. Dedecek, M. J. Lucero, C. B. Li, F. Gao, P. Klein, M. Urbanova, Z. Tvaruzkova, P. Sazama, S. Sklenak. *J. Phys. Chem. C* **115**, 11056 (2011).
- [47] K. Jisa, J. Novakova, M. Schwarze, A. Vondrova, S. Sklenak, Z. Sobalik. *J. Catal.* **262**, 27 (2009).